Applied Catalysis A: General 411–412 (2012) 77–86

Contents lists available at SciVerse ScienceDirect

Applied Catalysis A: General

journal homepage: www.elsevier.com/locate/apcata

Acid catalyzed organic transformations by heteropoly tungstophosphoric acid supported on MCM-41

Abd El Rahman S. Khder[a,b,*], Hassan M.A. Hassan[a,c], M. Samy El-Shall[a,**]

[a] Department of Chemistry, Virginia Commonwealth University Richmond, VA 23284-2006, United States
[b] Department of Chemistry, Mansoura University, Mansoura, Egypt
[c] Department of Chemistry, Faculty of Science, Suez Canal University, Suez, Egypt

ARTICLE INFO

Article history:
Received 23 July 2011
Received in revised form 10 October 2011
Accepted 15 October 2011
Available online 20 October 2011

Keywords:
Solid acid catalyst
MCM-41
Heteropoly acid
Pechmann
Esterification
Friedel–Crafts acylation reactions

ABSTRACT

In this work, solid acid catalysts of the Keggin-type 12-tungstophosphoric acid ($H_3PW_{12}O_{40}$, HPW) incorporated within the mesochannels of MCM-41 are prepared through a simple and effective impregnation method. The catalysts are characterized by various techniques such as XRD, FTIR, TEM, N_2 adsorption and thermal analysis. The surface acidities are measured by non-aqueous titration of *n*-butyl amine in acetonitrile and FTIR spectra of chemisorbed pyridine. The acidity and the textural parameters of the nanocomposites can be controlled simply by changing the loading of HPW on the MCM-41. The results indicate that the surface saturation coverage of MCM-41 is reached with 60 wt% HPW. The high saturation coverage is indicative of the well-dispersion of HPW within the mesochannels of MCM-41. The catalytic activities of the HPW/MCM-41 catalysts for the Pechmann, esterification reaction and Friedel–Crafts acylation reactions are studied in detail. Both the surface acidity and the catalytic activity sharply increase with the modification of MCM-41 by HPW. The sample with 60 wt% HPW shows the highest acidity and catalytic activity. The reusability tests of the catalysts show that the catalysts can be used several times without significant loss in activity. The HPW/MCM-41 catalysts have great potential for applications as commercial catalysts in promoting acid-catalyzed organic transformations under environmental friendly conditions and processes.

1. Introduction

In recent years, environmental considerations have raised strong interest in the development of economically feasible materials and processes to eliminate the use of harmful substances and the generation of toxic waste materials. In this respect, heterogeneous catalysis can play a key role in the development of environmentally benign processes particularly in the petroleum and chemical industries. For example, the substitution of liquid acid catalysts by efficient solid materials could contribute towards this goal. Highly porous molecular sieves such as MCM-41 provide an attractive possibility for the development of highly active solid acid catalysts [1,2]. MCM-41 is a promising support because of its large surface area (~1000 m^2/g), high thermal stability and large pore size (1.5–8 nm) [1–5]. However, MCM-41 lacks Brønsted acid sites and exhibits only weak hydrogen-bonded type of sites [6–8]. For MCM-41 to be used as a catalyst or catalyst support in acid-catalyzed reactions Brønsted acid sites need to be created and the acid strength must be enhanced. The acidity of MCM-41 can be increased by surface modification, through the introduction of strong acid species such as sulfate ions [9], sulfated zirconia [10] or heteropoly acids with Keggin-type structures [11,12], either on the surface or within the inner channels of MCM-41. This can result in creating Brønsted acid sites which can lead to a significant improvement in the acid strength of MCM-41.

Heteropoly solid acids with stable and strongly acidic properties, such as 12-tungstophosphoric acid ($H_3PW_{12}O_{40}$, HPW) have attracted much attention because of their strong acidity, high oxidation potential and redox characteristics which offer applications as Brønsted acid and redox catalysts [13–22]. Indeed, HPW supported on various materials has demonstrated high catalytic activity as an acid and oxidation catalyst for a variety for organic transformations including oxidative dehydrogenation of alkanes, olefin oxidation to epoxides, hydroisomerization and esterification reactions [13,16–18,23,24]. The choice of the support can overcome the major limitations of HPW which include low surface area of 5–10 m^2/g, low thermal stability and poor porosity [13–16]. For example, HPW clusters with diameters ~1.2 nm can be introduced inside the MCM-41 large pores of 2–8 nm, thus

* Corresponding author at: Department of Chemistry, Mansoura University, Mansoura, Egypt. Tel.: +20 010 6491649.
** Corresponding author at. Tel.: +1 804 828 3518.
E-mail addresses: askhder2244@yahoo.com (A.E.R.S. Khder), mselshal@vcu.edu (M.S. El-Shall).

0926-860X/$ – see front matter © 2011 Elsevier B.V. All rights reserved.
doi:10.1016/j.apcata.2011.10.024

allowing for a significant increase in the surface area of the HPW with a possible increase in its thermal stability, in addition to creating Brønsted acid sites within the MCM-41 support [4]. The large pore sizes of MCM-41 play a major role in overcoming the problem of the obstruction of bulky organic molecules resulting from the small pore volume of HPW. Therefore, HPW supported on MCM-41 can provide a potential solid acid catalyst with high activity and thermal stability.

Here, we report the preparation of MCM-41 with different loadings of the Keggin-type 12-tungstophosphoric acid (HPW) nanocrystals incorporated within the mesochannels of MCM-41 through a simple and effective impregnation method. The resulting catalyst materials have been characterized by various techniques including XRD, FTIR, TEM, thermal analysis, N_2 adsorption, and non-aqueous titration. The activity of these catalysts towards three different acid-catalyzed organic reactions has been extensively investigated under solvent-free conditions. The studied reactions include the Pechmann, esterification and Friedel–Crafts acylation reactions. The Pechmann reaction is one of the most widely used methods for the preparation of substituted coumarins since it proceeds from simple starting materials and results in good yields of a variety of substituted coumarins [25,26]. These compounds are important for a wide range of applications including fragrances, pharmaceuticals, food additives, cosmetics, tunable dye lasers, and others. Esterification is one of the fundamental reactions in organic syntheses. However, most of the reported procedures for the synthesis of esters require the use of sulfuric acid, hydrochloric acid, and toxic chemicals such as dimethyl sulfate, and/or methyl iodide which are environmentally hazardous [27,28]. Replacement of these acids by a solid acid catalyst such as HPW supported on MCM-41 would result in a simplified product recovery and elimination or reduction of undesirable waste streams. Friedel–Crafts acylation of aromatic compounds is an important reaction which is usually used in fine chemical and pharmaceutical industries [29,30]. The development of active and selective heterogeneous catalysts for these reactions is an important goal since the current efficient catalysts suffer from leaching of the active metal and behaving similar to homogeneous catalysts which cannot be regenerated. In this work, we demonstrate the successful applications of the prepared HPW–MCM-41 catalyst for three classes of acid-catalyzed reactions, and provide detailed information on the stability of the catalyst and the effect of reaction parameters on conversion and product selectivity. The results suggest that highly efficient HPW catalysts supported on MCM-41 can provide significant advances in the development of environmentally benign processes in the chemical industry.

2. Experimental

2.1. Preparation of catalysts

The original method for the preparation of MCM-41 was first proposed by Beck et al. [1]. However, the method used here is based on the modifications introduced in the original method to conduct the synthesis in mild conditions in terms of temperature and amount of surfactant amount. In a typical synthesis [31], 1.988 g of cetyl trimethyl ammonium bromide (CTAB, 98%, Sigma) was dissolved in 120 g of water at room temperature. After complete dissolution, 8 ml of aqueous NH_3 (32% in water, Merck) was added to the above solution. Then 10 ml of tetraethyl orthosilicate (TEOS, 99%, Flouka) was added to the solution under vigorous stirring. The hydrolysis of TEOS takes place during the first 2 min at room temperature (the solution becomes milky and slurry) whereas the condensation of the mesoporous hybrid material is achieved after 1 h of reaction. The material was then filtered and allowed to dry under static air at 80 °C for 12 h. The mesoporous material was finally obtained by calcination of the hybrid structure at 550 °C for 4 h.

HPW was supported on MCM-41 by an impregnation method. One gram of calcined MCM-41 was dispersed under vigorous stirring into a solution of the desired amount of HPW in 20 ml of water for 4 h. After removing the water by evaporation, the sample was dried at 110 °C over night in an oven and subsequently calcined at 350 °C for 4 h in a muffle furnace.

2.2. Characterization

X-ray powder diffraction patterns of samples were determined using an X'Pert Philips Materials Research Diffractometer. The patterns were run with copper radiation (Cu Kα, λ = 1.5405 Å) with the second monochromator at 45 kV and 40 mA with a scanning speed of 2° in 2θ/min. FT-IR spectra of calcined samples were recorded by using Nicolet-Nexus 670 FTIR spectrophotometer (4 cm^{-1} resolution and 32 scans) in dried KBr (Sigma) pellets and a measuring range of 400–4000 cm^{-1}. Transmission electron microscope (TEM) images and the particle size were obtained using a Jeol JEM-1230 operated at 120 kV. For TEM images the sample powder was dispersed in methanol by using ultrasonic radiation for 10 min and a drop of the suspension was placed onto the carbon-coated grids. The thermal stability of the samples was studied using TA thermal analyzer (DSC Q200 and TGA Q5000). The adsorption isotherms and the specific surface area (S_{BET}) of the various catalysts were determined from nitrogen adsorption studies conducted at −196 °C using Quantachrom Nova Sorbimetric system. The total acidity of the solid samples was measured by means of potentiometric titration [32,33]. The solid (0.05 g) was suspended in acetonitrile (Merck), and agitated for 3 h. Then the suspension was titrated with 0.05 N *n*-butylamine (Merck) in acetonitrile at 0.05 ml/min. The electrode potential variation was measured with an Orion 420 digital A model by using a double-junction electrode. Lewis and Brønsted acid sites present on the surface of the catalyst were determined with FT-IR spectra of adsorbed pyridine. Prior to the pyridine adsorption [34], small portions of the calcined samples were degassed under vacuum at 200 °C for 3 h followed by suspending in dry pyridine. Then, the excess pyridine was removed by evaporation. The FT-IR spectra of the pyridine-adsorbed samples were carried out using Nicolet-Nexus 670 FTIR spectrophotometer by mixing 0.005 g of the sample with 0.100 g KBr.

2.3. Catalytic activity

In all experiments the catalysts were activated at 200 °C for 2 h. The reactions were carried out in a 25 ml round bottom flask fitted with a condenser. The temperature of the reactions was maintained using an oil bath.

2.3.1. Synthesis of 7-hydroxy-4-methyl coumarin by Pechmann reaction

In a typical run, a mixture of resorcinol (10 mmol), ethyl acetoacetate (20 mmol) and activated catalyst (0.1 g), were magnetically stirred and heated to attain the reaction temperature (120 °C) for 1 h. After completion of the reaction, the reaction mixture was transferred into 10 ml of ethanol and stirred for 15 min. The catalyst was removed from the reaction mixture by simple filtration. The product sample was identified by GC–MS (HP GCD system equipped with EID) analysis. The ethanolic solution was heated to evaporate the solvent and subsequently the residue is recrystallized to afford 7-hydroxy-4-methyl coumarin. The yield of 7-hydroxy-4-methyl coumarin was obtained as follows:

Yield (wt%) = (Obtained weight of product) × 100/(Theoretical weight of product).

2.3.2. Esterification of acetic acid with n-octanol

The esterification reaction was carried out using 0.05 g of the catalyst. In a typical run, a mixture of 2 mmol of acetic acid (Aldrich, 99.8%) and 2 mmol of n-octanol (Aldrich, 98%) were magnetically stirred and heated to attain the reaction temperature (80 °C) for 1 h. Then the reaction mixture was filtered and the products were analyzed by means of GC–MS (HP GCD system equipped with EID). The yield was defined as the percentage of octyl acetate formed and calculated based on gas chromatographic analysis.

2.3.3. Friedel–Crafts acylation of anisole with acetic anhydride

In a typical run, a mixture of anisole (20 mmol), acetic anhydride (5 mmol) and activated catalyst (0.1 g), were magnetically stirred and heated to attain the reaction temperature (120 °C) for 1 h. After completion of the reaction, the catalyst was removed from the reaction mixture by centrifugation. Then, the reaction mixture was analyzed using GC–MS (HP GCD system equipped with EID). The main products are the *para*-methoxyacetophenone (*p*-MAP) and the *ortho*-methoxyacetophenone (*o*-MAP).

The conversion was calculated based on gas chromatographic analysis of the unconsumed acetic anhydride. The selectivity to each isomer was calculated based on the following:

% Selectivity to *p*-MAP = 100 × (peak area of *p*-MAP)/(peak area of *p*-MAP + peak area of *o*-MAP).

3. Results and discussion

3.1. Characterization of HPW catalyst supported on MCM-41

Fig. 1(A) displays the XRD patterns of the as-prepared and calcined MCM-41 before and after the incorporation of different weight percentage loadings of HPW namely, 20%, 30%, 40% and 70%. The XRD pattern of MCM-41 has four peaks that could be indexed to (1 0 0), (1 1 0), (2 0 0) and (2 1 0) reflections, which correspond to a well ordered hexagonal pore system [1,2]. The intensities of the diffraction peaks increase significantly after calcination, which must be related to the removal of the occluded surfactant molecules during the calcination process resulting in the enhancement of the structural ordering [35]. The 100 reflection of the MCM-41 is still observed after the HPW loading although the intensity of the diffraction peak becomes broader and weaker as the HPW loadings increases up to 60 wt%. This suggests that the mesoporous structure of the MCM-41 remains almost unchanged upon the HPW loading but the long-range order is significantly decreased. Although, the presence of HPW usually decrease long-range order of MCM-41 [36,37], but little explanation regarding this phenomenon was discussed. We studied the stability of MCM-41 under acidic conditions, in water and in presence of WO_3; the calcined MCM-41 material was stirred overnight in 0.1 M HCl, water and ammonium para tungstate (50 wt% WO_3/MCM-41) solutions followed by drying and calcination at 350 °C. The obtained XRD scans are shown in Supplementary Fig. S1. The main reflection at ($d_{(1\,0\,0)}$) of MCM-41, under all conditions was decreased. However, in presence of WO_3 much intensity decrease and broader reflection of ($d_{(1\,0\,0)}$) peak was observed. The results proved that MCM-41 is readily hydrolyzed under acidic conditions and becomes broader due to radiation absorption by the tungsten oxide. It is assumed that the severe reflection of MCM-41 in presence of HPW gradual hydrolysis in acidic medium and is mainly due to radiation absorption by the tungsten element present in HPW.

The absence of diffraction peaks due to the crystalline HPW phase in the diffraction patterns of the MCM-41 with HPW loadings up to 60 wt% (Fig. 1(B)) suggests that HPW is well dispersed within the support. This result is not surprising since the MCM-41 has a pore size higher than HPW nanocrystals, HPW are expected to be present inside the pores as well as on the MCM-41 surface. However, with loadings above 60 wt%, the reflections from the HPW crystals at $2\theta = 10.3°$, 14.5° and 18.0° are observed indicating poor dispersion or agglomeration of the HPW crystals at loading above 60 wt%.

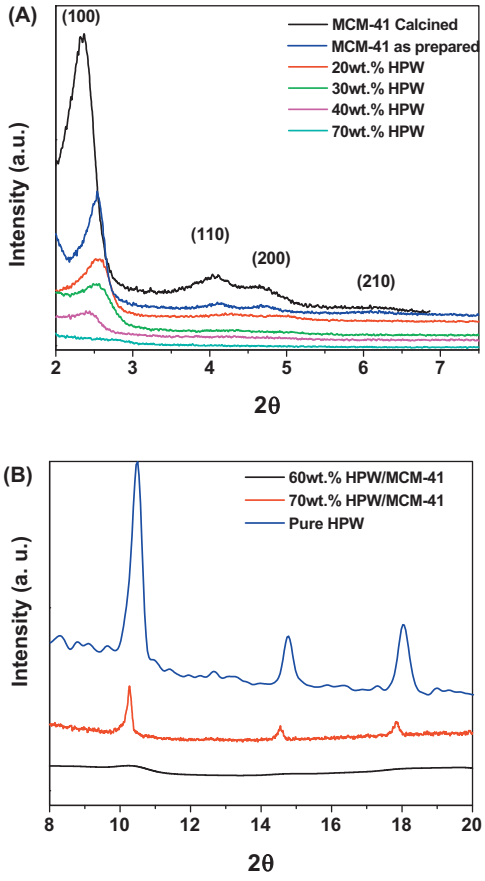

Fig. 1. (A) Low-angle XRD diffraction patterns of MCM-41 and HPW/MCM-41 samples. (B) XRD diffraction patterns of pure HPW, 60 wt% HPW/MCM-41, and 70 wt% HPW/MCM-41.

TEM images of MCM-41 with different magnifications are shown in Fig. 2(A). Periodic structures can be observed in the high magnification images indicating the high quality and long range order of the hexagonal MCM-41 materials. TEM images of the 20 wt% and 70 wt% HPW/MCM-41 are shown in Fig. 2(B). In the presence of HPW, darker spots appear in the TEM images of the MCM-41 which could be attributed to some HPW nanocrystals within the pores and/or on the surface of the MCM-41 crystals. No evidence for aggregation of the HPW nanocrystals could be found in the MCM-41 samples with HPW loading percentage <60 wt%. However, in the case of 70 wt% HPW/MCM-41 larger dark spots are observed on the surface which could be due to formation of multilayers of HPW on the surface of the MCM-41 crystals consistent with the XRD results shown in Fig. 1(B).

The supported HPW-MCM-41 samples were analyzed by FTIR in order to confirm the presence of the Keggin anion on the MCM-41. The $PW_{12}O_{40}^{3-}$ Keggin anion structure consists of a PO_4 tetrahedron surrounded by four W_3O_9 groups formed by edge-sharing octahedra. These groups are connected to each other by corner-sharing oxygen [38]. This structure gives rise to different types of oxygen atoms, being responsible for the fingerprint IR bands of the Keggin anion between 1100 and 500 cm^{-1}. The FTIR

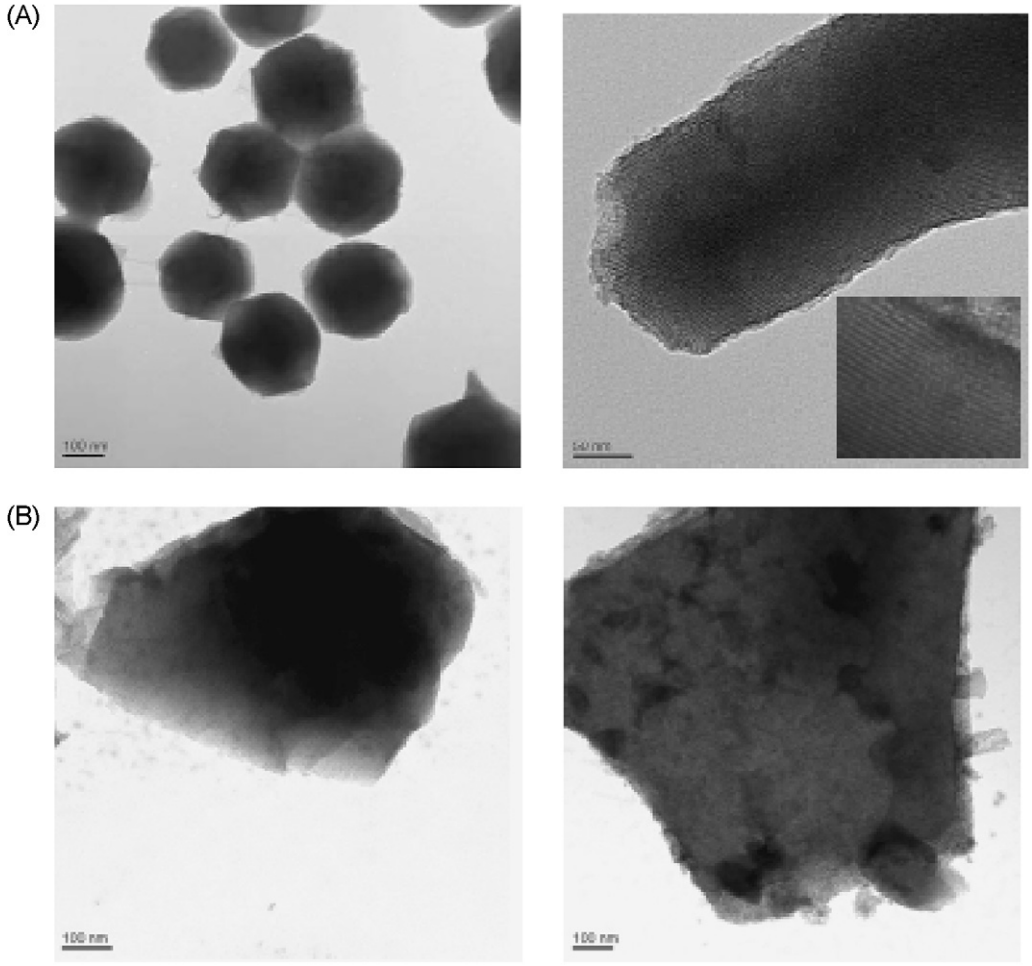

Fig. 2. TEM images of (A) pure MCM-4 and (B) 20 wt% HPW/MCM-41 (left), 70 wt% HPW/MCM-41 (right).

spectra of HPW with different loading percentages on MCM-41 are presented in Fig. 3. Bulk HPW shows five characteristic bands in the region 1100–500 cm^{-1}, observed at 1081, 982, 889, 797 and 595 cm^{-1}, which can be assigned to the stretching vibrations of P–O, W=O_t, W–O_c–W, W–O_e–W and the bending vibration of P–O, respectively. The MCM-41 is characterized by a broad band around 1300–1000 cm^{-1} assigned to an asymmetric stretching mode of Si–O–Si. This strong framework band of MCM-41 at 1090 cm^{-1} is not observed if the crystalline organization of MCM-41 is lost [37]. Another band at 807 cm^{-1} is due to the symmetric stretching vibration of the rocking mode of Si–O–Si [39]. The band at 970 cm^{-1} is assigned to the presence of Si–OH symmetric stretching vibration.

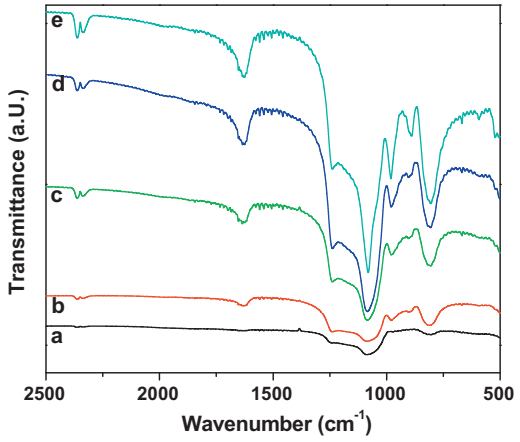

Fig. 3. FTIR spectra of (a) MCM-41, (b) 50 wt% HPW/MCM-41, (c) 60 wt% HPW/MCM 41, (d) 70 wt% HPW/MCM-41 and (e) bulk HPW.

The spectra displayed in Fig. 4 show clearly that the small bands at 982 cm^{-1} and 889 cm^{-1} became more evident with increasing the HPW loading on MCM-41. Moreover, the intensity of the MCM-41 band at 807 cm^{-1} gradually increases with the HPW loading due to the overlap with the HPW band at 797 cm^{-1}. These characteristic peaks of the Keggin ion confirm the presence and the stability of HPW into the MCM-41 framework.

The N_2 adsorption isotherms and pore size distributions of pure MCM-41 and several HPW samples with different loading percentages on MCM-41 are shown in Fig. 4(A) and (B). Table 1 lists the textural properties of pure MCM-41 and the supported HPW/MCM-41 [36,40]. These properties include $d_{(100)}$ (the d-spacing of the 100 diffraction in Å), $I_{(100)}$ (the intensity of the 100 diffraction), a_o (unit cell in nm), S_{BET} (BET surface area in m^2/g), pore volume in cc/g, and pore diameter in nm.

The adsorption isotherm of the parent MCM-41 mesoporous material displayed in Fig. 4(A) could be assigned to type IV isotherm. The HPW supported samples show a drop in the adsorption condensation region, at P/P^o = 0.2–0.4. The pore size distribution of pure and loaded MCM-41 shows a unique peak centered at about 35 Å diameters. It is evident that the pore volume and the specific surface area of the loaded sample are much lower compared to that of the parent MCM-41. This is consistent with previous results which indicate that the surface area of MCM-41 continuously decreases with

Table 1
Textural properties of the HPW/MCM catalysts.

	$d_{(100)}$(Å)	$I_{(100)}$	Unit cell, a_o (nm)	S_{BET} (m^2/g)	Pore volume (cc/g)	Pore diameter (nm)
Dried MCM-41	40.04	482	4.62	–	–	–
Calcined MCM-41	34.29	1311	3.96	982	0.85	3.5
20 wt% HPW/MCM-41	31.19	310	3.60	846	0.81	3.5
30 wt% HPW/MCM-41	34.25	252	3.95	789	0.70	3.6
40 wt% HPW/MCM-41	33.09	147	3.82	723	0.59	3.6
50 wt% HPW/MCM-41	33.18	68	3.83	604	0.52	3.5
60 wt% HPW/MCM-41	34.03	164	3.93	472	0.35	3.4
70 wt% HPW/MCM-41	31.61	33	3.65	219	0.22	3.5

increasing the heteropolyacid content [36,40]. The reduction in the pore volume and surface area after loading could be due to the fact that the HPW is deposited inside the mesochannels and is well-dispersed on the surface of the hexagonally ordered mesoporous MCM-41 support.

The thermal stability of HPW and HPW loaded on MCM-41 samples was studied using DSC of the uncalcined samples. The catalytic activity and structure of the heteropolyacids mainly depend upon its degree of hydration. Thus, TGA and DSC scans were obtained for the hydrated bulk HPW sample as shown in Fig. 5(A). The bulk hydrated $H_3PW_{12}O_{40}{\cdot}xH_2O$ shows three stage weight loss processes: (a) the first peak observed at a temperature below 140 °C (9.11%) corresponds to the loss of 15 molecules of the physisorbed water; (b) a peak in the temperature range of 150–280 °C (2.52%), which accounts for the loss of 6 H_2O molecules per Keggin unit; (c) a peak in the range of 370–580 °C (1.42%) due to the loss of 1.5 H_2O molecules corresponding to the loss of all acidic protons and the beginning of decomposition of the Keggin structure [41]. These results indicate that the hydrated HPW contains 21 H_2O molecules per Keggin unit. Another exothermic effect at 605 °C is due to the decomposition of Keggin anion ($PW_{12}O_{38.5}$) to form both phosphorous and tungsten oxides [42]. HPW showed that the decomposition takes place without appreciable weight loss, which may support the decomposition of Keggin anion ($PW_{12}O_{38.5}$) to the corresponding oxides (0.5 P_2O_5 and 12 WO_3).

Fig. 5(B) displays some selected DSC curves of the prepared samples. The samples show endothermic peaks between 150 and 260 °C, corresponding to removal of the adsorbed water molecules. The significant result is the absence of the exothermic peak due to the decomposition of HPW in the supported MCM-41 samples with up to 60 wt% HPW. This may be due to the high dispersion of HPW into MCM-41 pores. On the other hand, a weak exothermic peak is observed at 605 °C in the DSC curve of the 70 wt% HPW loaded on MCM-41 indicating the decomposition of the aggregated HPW crystals on the surface of the support.

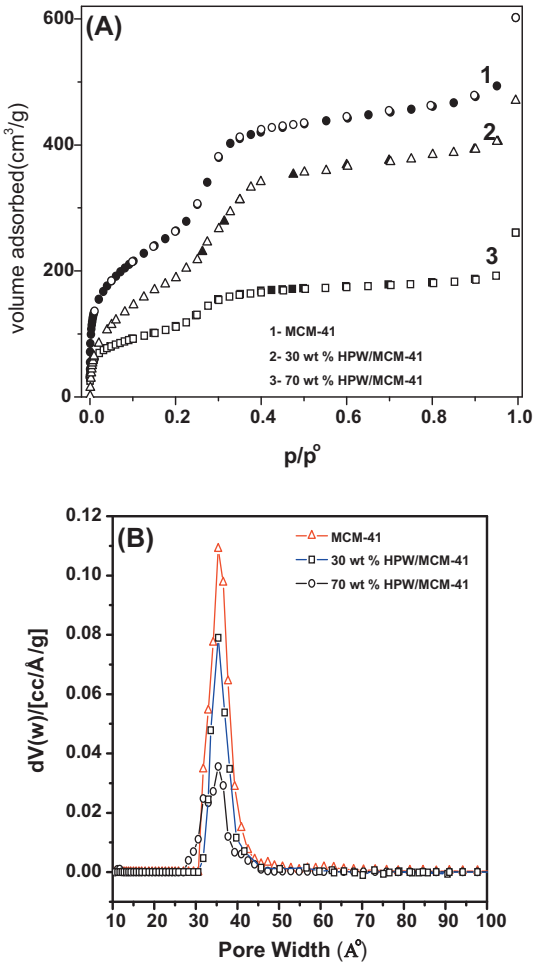

Fig. 4. (A) Adsorption–desorption isotherms of N_2 at −196 °C over MCM-41, 30 wt% HPW/MCM-41 and 70 wt% HPW/MCM-41. (B) Pore size distribution curves of MCM-41, 30 wt% HPW/MCM-41 and 70 wt% HPW/MCM-41.

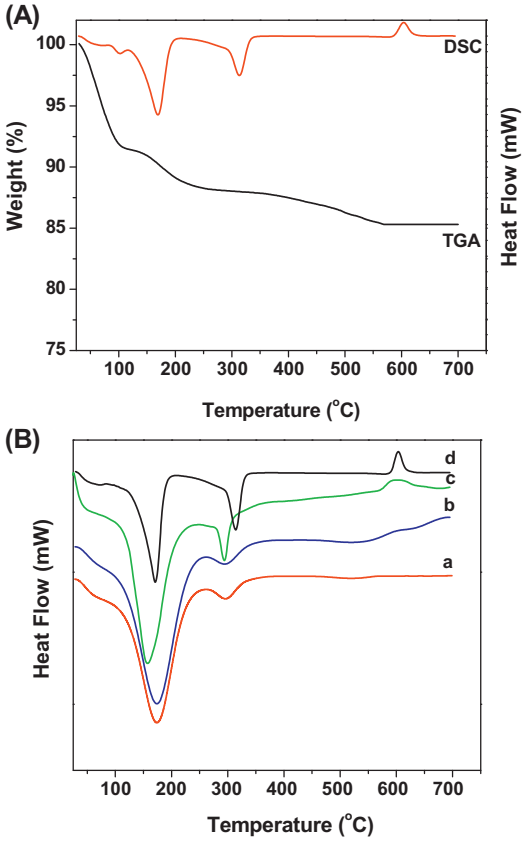

Fig. 5. (A) TGA–DSC profiles of pure HPW. (B) DSC scans of: (a) 50 wt% HPW/MCM-41, (b) 60 wt% HPW/MCM-41, (c) 70 wt% HPW/MCM-41 and (d) bulk HPW.

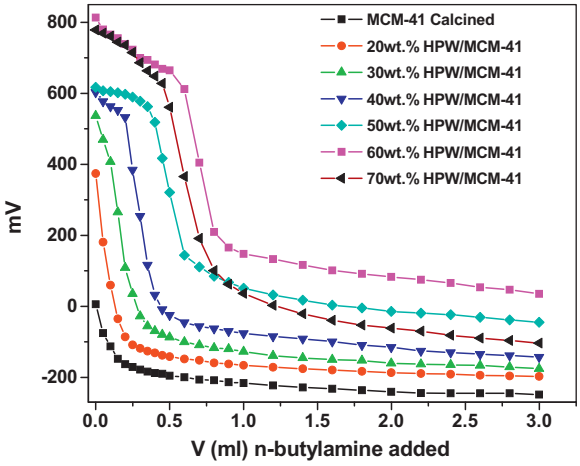

Fig. 6. Potentiometric titration curves of *n*-butyl amine in acetonitrile for the prepared catalysts.

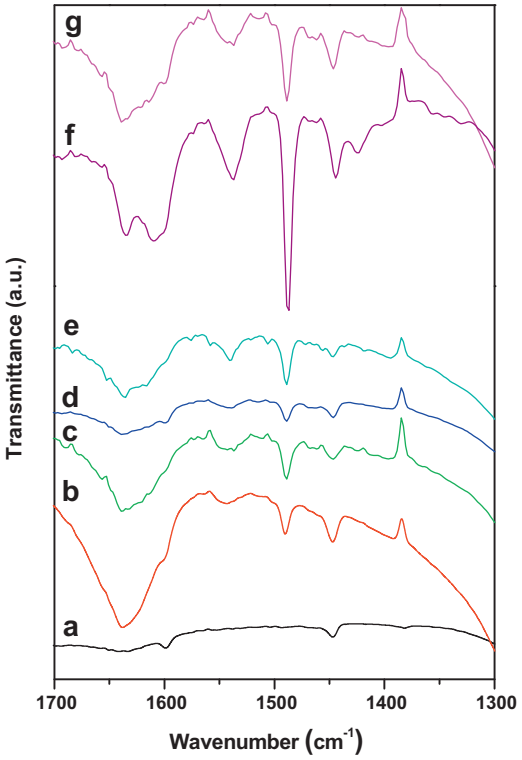

Fig. 7. FTIR spectra of pyridine adsorbed on: (a) MCM-41, (b) 20 wt% HPW/MCM-41, (c) 30 wt% HPW/MCM-41, (d) 40 wt% HPW/MCM-41, (e) 50 wt% HPW/MCM-41, (f) 60 wt% HPW/MCM-41, and (g) 70 wt% HPW/MCM-41.

Generally, the thermal stability of heteropoly acids loaded on different supports depends on the type of the support, the HPW loading and the conditions of pretreatment. Acidic or neutral carriers such as SiO_2 [43], active carbon [44], and acidic ion exchange resin [45] are suitable as supports. Basic solids such as MgO [46] tend to decompose HPW due to the strong interaction with HPW. Wu et al. reported that the thermal stability of 12-tungstogermanic acid loaded on silica is lower than that of pure 12-tungstogermanic acid due to strong interactions with the support [47]. On the other hand SiO_2-supported molybdenum HPWs, retain the Keggin structure at high loadings but decompose at very low loadings due to strong interactions with surface silanol groups [48]. In the present work, with loadings up to 60 wt% of HPW on MCM-41, HPW forms finely dispersed nanocrystals inside the pores and on the MCM-41 surface. However, when the HPW content exceeds the monolayer coverage (as evident from XRD), this leads to the formation of polylayers or agglomeration of HPW on the MCM-41 surface. The surface excess concentration of HPW is accompanied by an exothermic effect at 605 °C observed in the sample loaded with 70 wt% HPW. This indicates that the thermal stability of HPW on MCM-41 seems to be comparable to that of pure HPW. This may be due to weak interactions between HPW and the support as a result of the weakly acidic nature of MCM-41.

3.2. Surface acidity measurements

The acidity of the solids was characterized by potentiometric titration with *n*-butylamine. Using this technique, it is possible to estimate the strength and the total number of acid sites present in the solids. As a criterion to interpret the results, it was suggested that the initial electrode potential (E_i) indicates the maximum acid strength of the sites and the value of mequiv. amine/g solid where the plateau is reached indicates the total number of acid sites [49,50]. Nevertheless, the end point of the titration given by the inflexion point of the curve is a good measure to carry out a comparison of the acidity of the different samples. On the other hand, the acid strength of acid sites may be classified according to the following scale: $E_i > 100$ mV (very strong sites), $0 < E_i < 100$ mV (strong sites), $-100 < E_i < 0$ mV (weak sites) and $E_i < -100$ mV (very weak sites) [51].

The titration curves of the catalysts are displayed in Fig. 6. While the MCM-41 support exhibits acid sites with an E_i value of 7 mV, the supported HPW samples exhibit much higher values (as expected) in the range of 374–813 mV (Table 2). The number of acid sites determined by potentiometric titration increases in parallel with the increase of TPA content up to 60 wt%, then decreases with further increase in HPW content. Additionally, the acid strength of the catalysts changes in the same way. Pure MCM-41 surface has Si–OH (silanol groups) which are weakly acidic in nature. When these silanol groups replaced with stronger acidic sites of HPW the number and strength of the acid sites will increase. As the coverage of MCM surface increases by HPW, the number and strength of acid sites will increase. The sample with the highest HPW content (70 wt% above surface saturation coverage) shows loss of acidity and acid strength probably due to agglomeration (Keggin–Keggin interactions) of the crystalline HPW on the surface of the support as detected by XRD and TEM.

The Brønsted (B) and Lewis (L) acidic sites in the supported HPW catalysts can be characterized using pyridine as a probe molecule. The FTIR spectra of pyridine adsorbed on the catalysts are shown in Fig. 7. All the catalysts contain Lewis (L) acid sites and Brønsted (B) acid sites, as indicated by the adsorption bands at 1444 cm^{-1} (L), 1600 cm^{-1} (L), 1542 cm^{-1} (B) and 1640 cm^{-1} (B) [52]. In addition, the band at 1488 cm^{-1} indicates the formation of the adjacent L and B acid sites. In comparison with the support (MCM-41), the nature of the acidity of the HPW supported catalysts shows the following changes:

(1) The FTIR spectrum of MCM-41 after the adsorption of pyridine shows bands at 1600 and 1448 cm^{-1} in agreement with results previously reported [53]. These bands are assigned to the adsorption of pyridine on weak L acid sites or to weakly hydrogen-bonded pyridine.
(2) Incorporation of HPW on MCM-41 and the adsorption of pyridine give rise to the development of both B and L acid sites. Bands assigned to the pyridinium ions are observed at 1542 and 1640 cm^{-1} and those associated with pyridine coordinated to Lewis (L) acid sites are observed at 1444 and 1600 cm^{-1}. In

Table 2
Acidic properties of the HPW/MCM-41 catalysts. E_i, initial electrode potential in mV, $I(B)_{1542}$ and $I(L)_{1444}$ are the intensity of the IR bands at 1542 cm^{-1} and 1444 cm^{-1} corresponding to pyridine adsorbed on Brønsted and Lewis acid sites, respectively.

	E_i	No. of acid sites in mequiv. g^{-1}	$I(B)_{1542}$	$I(L)_{1444}$	$I(B)/I(L)$
Dried MCM-41	–	–	–	–	–
Calcined MCM-41	+7	0.25	–	0.41	–
20 wt% HPW/MCM-41	+374	0.47	0.44	1.10	0.40
30 wt% HPW/MCM-41	+537	0.93	0.69	0.81	0.85
40 wt% HPW/MCM-41	+603	1.48	0.73	0.85	0.86
50 wt% HPW/MCM-41	+617	1.96	1.32	0.80	1.65
60 wt% HPW/MCM-41	+813	2.99	4.72	2.01	2.35
70 wt% HPW/MCM-41	+778	2.81	3.62	1.72	2.10

addition, the band at 1488 cm^{-1} indicates the formation of the adjacent L and B acid sites.

(3) The acidity varies depending on the amount of HPW loaded on the support. The intensity of B and L acid sites, obtained from the absorbance at 1542 and 1444 cm^{-1} and their corresponding B/L intensity ratios [51] are shown in Table 2. At low loading, the catalyst showed both Brønsted and Lewis acidities; with an increase in loading both Brønsted and Lewis acidities increase. On the other hand, the increase in the Brønsted acidity is much more than the Lewis acidity up to 60 wt% HPW at which the Brønsted acidity reaches a maximum (B/L = 2.35).

From the results of the acidity measurements it can be concluded that, the incorporation of HPW enhances the surface acidity and acid strength up to the monolayer coverage. Increasing in the HPW loading above 60 wt% decreases the surface acidity and acid strength due to agglomeration of the crystalline HPW, which prevents the accessibility of pyridine to the active sites.

3.3. Catalytic activity

The HPW/MCM-41 catalysts prepared were used as solid acid catalysts in three acid-catalyzed organic reactions namely, the Pechmann, esterification and Friedel–Crafts acylation reactions.

3.3.1. The Pechmann reaction

The reaction between resorcinol and ethyl acetoacetate was carried out using 0.1 g of the HPW supported catalyst (20–70 wt%) at 120 °C for 1 h. As shown in Fig. 8, the prepared catalysts exhibit high catalytic activity under the reaction conditions used. For the most active catalyst (60 wt% HPW), more than 96% of 7-hydroxy-4-methyl coumarin was obtained with 100% selectivity. Sudha et al. reported that, the formation of 7-hydroxy-4-methyl coumarin takes place through the chemisorption of the carbonyl group of ethyl acetoacetate on the Brønsted acid sites of the catalyst [54]. This is followed by a nucleophilic attack by resorcinol to form coumarin. A close examination of the B/L ratios (Table 2) and the catalytic activity results (Fig. 8) shows clearly that the sample with higher B/L ratio exhibits the maximum catalytic activity. The direct correlation between surface acidity (Brønsted acidity) and catalytic activity explains the role of HPW in enhancing the surface acidity and consequently the catalytic activity of the catalysts. Compared to other published work [54–56], our catalyst exhibits higher catalytic activity in a shorter reaction time, lower temperature and smaller amount of the catalyst. The reusability of the 60 wt% HPW/MCM-41 sample was checked with two consecutive syntheses of 7-hydroxy-4-methyl coumarins by using recovered samples after reactivation at 200 °C. The product yield in the two consecutive runs (95.4% and 93.8%, respectively) indicates excellent reusability with very little activity loss from the first run (96%).

3.3.2. Esterification reaction

The esterification reaction between acetic acid and n-octanol was carried out using 0.05 g of the catalyst at 80 °C for 1 h reaction time. The main products of the reaction were octylacetate with high selectivity and a mixture of 2- and 4-octene with low selectivity. As shown in Fig. 9, the most active catalyst (60 wt% HPW/MCM-41) shows 100% yield with nearly 99% selectivity to octylacetate. Generally Brønsted acid sites catalyze esterification reactions, but according to other work esterification can also be catalyzed by Lewis acid sites typically using metal ions in low coordination states [57,58]. However, most of the literature work shows that both Brønsted and Lewis acid sites are responsible for catalyzing the esterification reaction [59,60]. Moreover, the formation of alkenes as side products of the reaction supports the idea that the mechanism of the reaction proceeds via a protonated alcohol intermediate [61]. This means that the reaction proceeds by

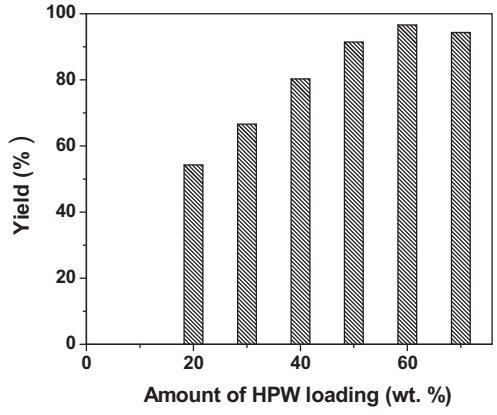

Fig. 8. Influence of HPW content in HPW/MCM-41 catalysts on yield of 7-hydroxy-4-methyl coumarin (reaction condition: resorcinol/EAA, 1:2; reaction time, 1 h; temperature, 120 °C; catalyst weight, 0.1 g).

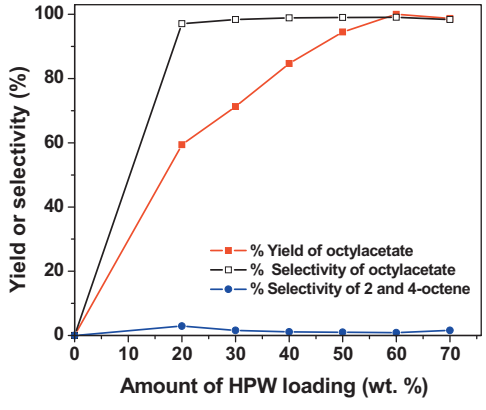

Fig. 9. Influence of HPW content in HPW/MCM-41 catalysts on yield and selectivity of octyl acetate and on selectivity to octyl acetate or to 2 and 4 octene (reaction condition: acetic acid/n-octanol, 1:1; reaction time, 1 h; temperature, 80 °C; catalyst weight, 0.05 g).

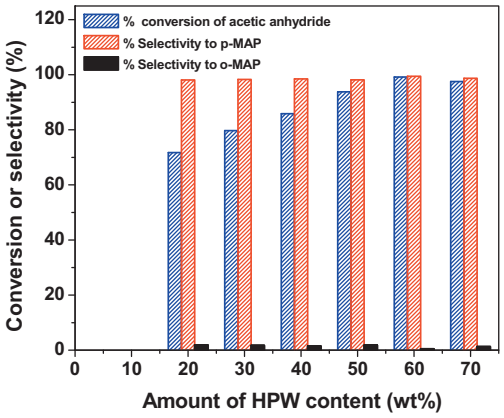

Fig. 10. Influence of HPW content in HPW/MCM-41 catalysts on conversion of acetic anhydride (in %) and % selectivity to *p*-MAP and *o*-MAP (in %) (reaction condition: anisole/acetic anhydride, 4:1; reaction time, 1 h; temperature, 120 °C; catalyst weight, 0.1 g).

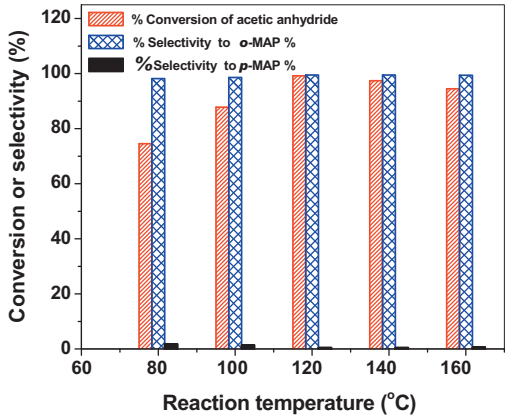

Fig. 11. Influence of reaction temperature on conversion of acetic anhydride (in %) and selectivity to *p*-MAP and *o*-MAP (in %) over 60 wt% HPW/MCM-41 catalyst (reaction condition: anisole/acetic anhydride, 4:1; reaction time, 1 h; catalyst weight, 0.1 g).

the adsorption of n-octanol over Brønsted and/or Lewis acid sites forming a protonated alcohol intermediate, which then reacts with acetic acid to form the corresponding ester and water.

The reusability of 60 wt% HPW/MCM-41 sample was also checked with two consecutive reactions by using the recovered sample after reactivation at 200 °C and resulting overall yield was 98.7 and 97.1%, respectively.

3.3.3. *Friedel–Crafts acylation reaction*

The Friedel–Crafts acylation of anisole using acetic anhydride was carried out using 0.1 g of the catalyst at 120 °C for 1 h (the optimum conditions). The main products obtained are *para*-methoxyacetophenone (*p*-MAP, major product) and the *ortho*-methoxyacetophenone (*o*-MAP, minor product).

Fig. 10 displays the catalytic activity of the catalysts prepared with different loadings of HPW (20–70 wt%) at 120 °C. It should be noted that pure MCM-41 did not show any catalytic activity for the acylation of anisole with acetic anhydride. However, loading MCM-41 with of 20 wt% HPW results in a sudden increase in the % conversion of acetic anhydride to around 70%. The % conversion of acetic anhydride further increases as HPW content increase up to maximum limit at 60 wt% HPW with 99.2%. A slight decrease in the % conversion of acetic anhydride is observed for the 70 wt% HPW catalyst. It is important to note that in all the different HPW loadings, the selectivity towards *p*-MAP between 98.1 and 99.5% in all the catalysts, which may indicate that this selectivity is independent of the number and strength of acidic sites.

Fig. 11 displays the effect of reaction temperature effect on the acetic anhydride conversion using the 60 wt% HPW/MCM-41 catalyst. Significant increase in the overall yield is observed with increasing temperature until 120 °C after which a slight decrease in the yield is observed. The slight decrease in conversion at high temperatures is probably due to the inhibiting effect of the *p*-MAP, which can be strongly adsorbed on the catalyst at higher conversion. A decrease in conversion at high temperatures was also observed in the acylation of toluene with acetic anhydride due to the strong adsorption of methylacetophenones [62].

The effect of the anisole to acetic anhydride molar ratio on the acetic anhydride conversion was studied using 0.1 g of 40, 60 and 70 wt% HPW loaded MCM-41 at 120 °C for 1 h, and the results are shown in Fig. 12. The conversion of acetic anhydride increases with increasing the concentration of anisole up to four times that of acetic anhydride and thereafter remains constant. Increasing conversion of acetic anhydride is attributed to the facile desorption of

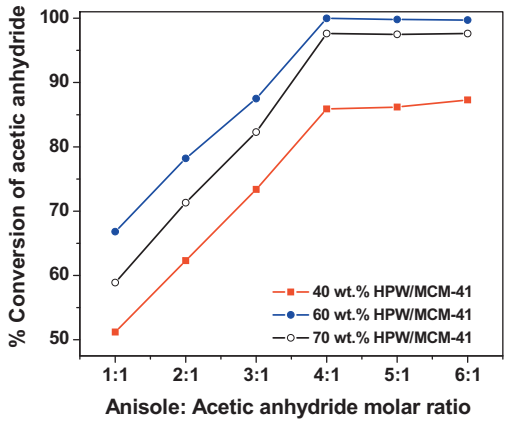

Fig. 12. Variation of the conversion of acetic anhydride with the anisole/acetic anhydride molar ratio HPW/MCM-41 catalysts (reaction time, 1 h; temperature, 120 °C; catalyst weight, 0.1 g).

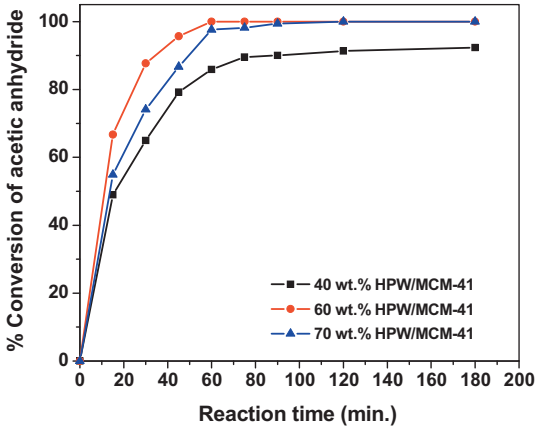

Fig. 13. Effect of reaction time on conversion of acetic anhydride (%) (reaction condition: anisole/acetic anhydride, 4:1; temperature, 120 °C; catalyst weight, 0.1 g).

acetic acid and *p*-MAP formed through the catalyst pores by the excess anisole as anisole is a self-solvent [63].

The effect of reaction time on the % conversion of acetic anhydride over 0.1 g of 40, 60 and 70 wt% HPW loaded MCM-41 keeping anisole: acetic anhydride molar ratio at 4:1 at 120 °C is shown in Fig. 13. It was found that the percentage of conversion of

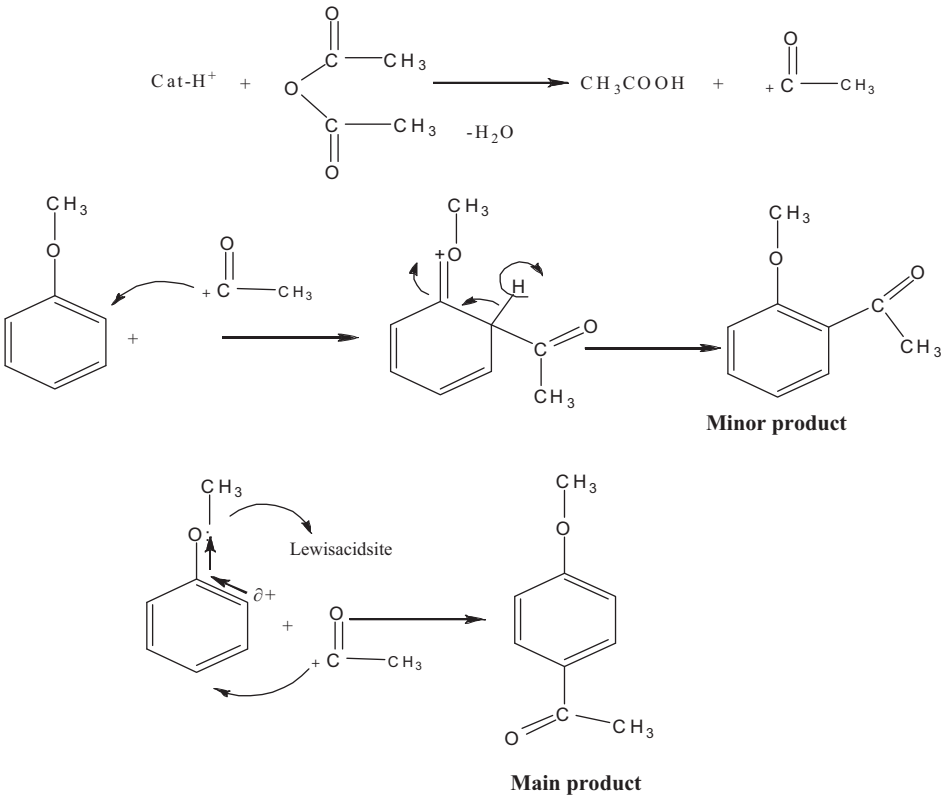

Scheme 1. Proposed reaction mechanism for the acylation of anisole with acetic anhydride in presence of Brønsted and Lewis acid sites.

acetic anhydride becomes maximum after 1 h and then remains almost constant with further increase of reaction time more than 3 h.

Recycling of the catalyst is an important aspect of any industrial process. For this purpose, reusability of the catalyst is tested by carrying out repeated runs of the reaction at 120 °C, keeping the reactants molar ratio (anisole/acetic anhydride) at 4:1. It was observed that no significant loss in the activity of the 40 wt% HPW/MCM-41 with increasing the number of cycles of the reaction. This could probably be due to irreversible adsorption of methylacetophenones on the catalyst active sites or loss of catalyst due to filtration and washing processes (Fig. 14).

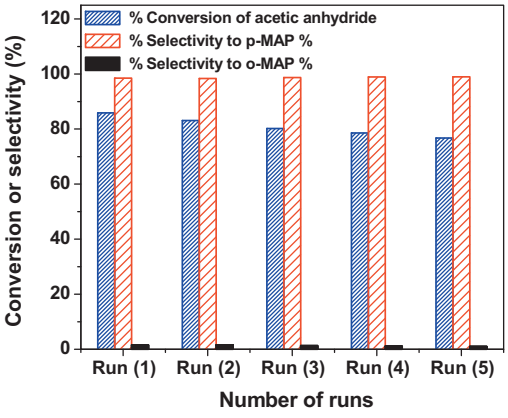

Fig. 14. Variation of conversion of acetic anhydride (%) or selectivity to *p*-MAP and *o*-MAP (%) with reusability, studied over 40 wt% HPW/MCM-41 catalyst (reaction condition: anisole/acetic anhydride, 4:1; reaction time, 1 h; temperature, 120 °C; catalyst weight, 0.1 g).

4. Reaction mechanism

The acylation reaction is an electrophilic substitution reaction where Brønsted acid sites are responsible for the generation of an $R–CO^+$ ion from the actyling agent. Thus the catalytic activity is expected to depend on the number and strength of the Brønsted acidity sites. The proposed mechanism (Scheme 1) for the acylation reaction implies the formation of an adsorbed acylium ion adsorbed on the active site by interaction of the acetic anhydride with a Brønsted acid site [64,65]. Then, the reaction between the adsorbed acylium ion and anisole in the liquid phase occurs to give the final products. Generally the acylation of anisole with acetic anhydride gives *p*-MAP with a high selectivity and *o*-MAP with a low selectivity. The formation of *p*-MAP with high selectivity could be due to steric hindrance which makes *p*-MAP more favorable than *o*-MAP. On the other hand, the Lewis acid sites may also play an important role as shown in Scheme 1. The Brønsted acid sites are responsible for the CH_3CO^+ formation while the Lewis sites favor the formation of the *para* substituted product [66]. The stronger the Lewis acid site the more electron deficient the *ortho* position and this could restrict the attack of the electrophile (CH_3CO^+) mostly to the *para* position thus leading to higher *para* selectivity.

5. Conclusions

The results of this study show that HPW loading has a notable effect on the acidity and catalytic activity of MCM-41. The mesoporous structure of MCM-41 is not affected much with the HPW loading up to 70 wt%. Higher loadings result in structural distortion of MCM-41 with considerable loss of the long range order. Both the surface acidity and the ratio of Brønsted to Lewis acidic sites of the HPW catalyst attain the maximum value at 60 wt% HPW loading. The catalytic activity of these catalysts in Pechmann,

esterification and Friedel–Crafts acylation reactions is significantly high thus suggesting the HPW/MCM-41 materials are potentially promising catalysts for acid-catalyzed organic transformations in environmentally friendly processes to supersede the use of conventional homogeneous HPW catalysts.

Acknowledgment

This work was supported by the National Science Foundation (CHE-0911146). We also thank the National Science Foundation (OISE-0938520) for the support of the "US-Egypt Advanced Studies Institute on Nanomaterials and Nanocatalysis for Energy, Petrochemicals and Environmental Applications" which facilitated the completion of this work. We gratefully acknowledge Dr. Victor Abdelsayed for the TEM work.

Appendix A. Supplementary data

Supplementary data associated with this article can be found, in the online version, at doi:10.1016/j.apcata.2011.10.024.

References

[1] J.S. Beck, J.C. Vartuli, W.J. Roth, M.E. Leonowicz, C.T. Kresge, K.D. Schmit, C.T.W. Chu, D.H. Olson, E.W. Sheppard, S.B. McCullen, J.B. Higgins, J.L. Schlenker, J. Am. Chem. Soc. 114 (1992) 10834–10843.
[2] C.T. Kresge, M.E. Leonowicz, W.J. Roth, J.C. Vartuli, J.C. Beck, Nature 359 (1993) 710–712.
[3] I.V. Kozhevnikov, K.R. Kloetstra, A. Sinnema, H.W. Zandbergen, H. Van Bekkum, J. Mol. Catal. A 114 (1996) 287–298.
[4] I.V. Kozhevnikov, A. Sinnema, R.J.J. Jansen, K. Pamin, H.V. Bekkum, Catal. Lett. 30 (1995) 241–252.
[5] P.R.S. Braga, A.A. Costa, J.L. Macedo, G.F. Ghesti, M.P. Souza, J.A. Dias, S.C.L. Dias, Microporous Mesoporous Mater. 139 (2011) 74–80.
[6] A. Corma, V. Fornes, M.T. Navarro, J.P. Pariente, J. Catal. 148 (1994) 569–574.
[7] V. Gusev, X.Yu. Feng, Z. Bu, G.L. Haller, J.A. O'Brien, J. Phys. Chem. 100 (1996) 1985–1988.
[8] A. Galarneau, D.D. Giscard, F. Di Renzo, F. Fajula, Catal. Today 68 (2001) 191–200.
[9] T. Okuhara, N. Mizuno, M. Misono, Appl. Catal. A 222 (2001) 63–77.
[10] S. Biz, M.L. Occelli, Catal. Rev. Sci. Eng. 40 (1998) 329–407.
[11] Y. Liu, L. Xu, B. Xu, Z. Li, L. Jia, W. Guo, J. Mol. Catal. A 297 (2009) 86–92.
[12] A.M. Alsalme, P.V. Wiper, Y.Z. Khimyak, E.F. Kozhevnikova, I.V. Kozhevnikov, J. Catal. 276 (2010) 181–189.
[13] I.V. Kozhevnikov, Chem Rev. 98 (1998) 171–198.
[14] N. Mizuno, M. Misono, Chem. Rev. 98 (1998) 199–217.
[15] C.L. Hill, C.M. Prossermccartha, Coord. Chem. Rev. 143 (1995) 407–455.
[16] J. Haber, K. Pamin, L. Matachowski, D. Mucha, Appl. Catal. A 256 (2003) 141–152.
[17] Y. Izumi, K. Hisano, T. Hida, Appl. Catal. A 181 (1999) 277–282.
[18] A.S. Khder, Appl. Catal. A 343 (2008) 109–116.
[19] Z. Zhu, W. Yang, J. Phys. Chem. C 113 (2009) 17025–17031.
[20] K. Zhu, J. Hu, X. She, J. Liu, Z. Nie, Y. Wang, C.H.F. Peden, J.H. Kwak, J. Am. Chem. Soc. 131 (2009) 9715–9721.
[21] K. Okumura, S. Ito, M. Yonekawa, A. Nakashima, M. Niwa, Top. Catal. 52 (2009) 649–656.
[22] X.K. Yang, L.F. Chen, J.A. Wang, L.E. Norena, O. Novaro, Catal. Today 148 (2009) 160–168.
[23] F. Zhang, C. Yuan, J. Wang, Y. Kong, H. Zhu, C. Wang, J. Mol. Catal. A 247 (2006) 130–137.
[24] F.M. Zhang, J. Wang, C. Yuan, X.Q. Ren, Catal. Lett. 102 (2005) 171–174.
[25] R. O'Kennedy, R.D. Thornes, Coumarins: Biology Applications and Mode of Action, Wiley, Chichester, 1997.
[26] M. Zabradnik, The Production and Application of Fluorescent Brightening Agents, Wiley, New York, 1992.
[27] G.A. Bardock, Fenaroli's Handbook of Flavor Ingredients, vol. 11, 3rd ed., CRC, 1994.
[28] S.K. Bhorodwaj, M.G. Pathak, D.K. Dutta, Catal. Lett. 133 (2009) 185–191.
[29] G.A. Olah, Friedel–Crafts and Related Reactions, Wiley-Interscience, New York, 1973.
[30] R.A. Sheldon, H.V. Bekkum, Fine Chemical Through Heterogeneous Catalysis, Wiley-VCH, Weinhein, 2000.
[31] P. Trens, M.L. Russell, L. Spjuth, M.J. Hudson, J. Liljenzin, Mater. Interface 41 (2002) 5220–5225.
[32] K.N. Rao, K.M. Reddy, N. Lingaiah, I. Suryanarayana, P.S. Sai, J. Prasad, Appl. Catal. A 300 (2006) 139–146.
[33] A.S. Khder, A.I. Ahmed, Appl. Catal. A 354 (2009) 153–160.
[34] H. Matsuhashi, H. Motoi, K. Arata, Catal. Lett. 26 (1994) 325–328.
[35] A. Maheswari, K. Shanthi, T. Sivakumar, S. Narayanan, Appl. Catal. A 245 (2003) 221–230.
[36] B.R. Jermy, A. Pandurangan, Appl. Catal. A 295 (2005) 185–192.
[37] A.G. Siahkali, A. Philippou, J. Dwyer, M.W. Anderson, Appl. Catal. A 192 (2000) 57–69.
[38] M. Hashimoto, G.N. Koyano, N. Mizuno, J. Phys. Chem. B 108 (2004) 12368–12374.
[39] Q.H. Xia, K. Hidajat, S. Kawi, Mater. Lett. 42 (2000) 102–107.
[40] J.C. Juan, J. Zhang, M.A. Yarmo, J. Mol. Catal. A 267 (2007) 265–271.
[41] A.V. Ivanov, T.V. Vasina, V.D. Nissenbaum, L.M. Kustov, M.N. Timofeeva, J.I. Houzvicka, Appl. Catal. A 259 (2004) 65–72.
[42] I.V. Kozhevnikov, J. Mol. Catal. A 262 (2007) 86–92.
[43] Y. Izumi, R. Hasebe, K. Urabe, J. Catal. 84 (1983) 402–409.
[44] Y. Izumi, K. Urabe, Chem. Lett. 5 (1981) 663–666.
[45] T. Baba, Y. Ono, Appl. Catal. A 22 (1986) 321–324.
[46] T. Matsuda, A. Igarashi, Y. Ogino, J. Jpn. Petrol. Inst. 23 (1980) 30–42.
[47] Q. Wu, S. Tao, H. Lin, G. Meng, Mater. Chem. Phys. 64 (2000) 25–28.
[48] K. Bruckman, M. Che, J. Haber, J.M. Tatibouet, Catal. Lett. 25 (1994) 225–240.
[49] D.O. Bennardi, G.P. Romanelli, J.C. Autino, L.R. Pizzio, Appl. Catal. A 324 (2007) 62–68.
[50] E.A. El-Sharkawy, A.S. Khder, A.I. Ahmed, Microporous Mesoporous Mater. 102 (2007) 128–137.
[51] P. Sharma, S. Vyas, A. Patel, J. Mol. Catal. 214 (2004) 281–286.
[52] E.F. Lopez, V.S. Escribano, M. Panizza, M.M. Carnasciali, G. Busca, J. Mater. Chem. 11 (2001) 1891–1897.
[53] A. Jentys, K. Kleestofer, H. Vinek, Microporous Mesoporous Mater. 27 (1999) 321–328.
[54] S. Sudha, K. Venkatachalam, S.V. Priya, J.H. Mabel, M. Palanichamy, V. Murugesan, J. Mol. Catal. A 291 (2008) 22–29.
[55] B. Tyagi, M.K. Mishra, R.V. Jasra, J. Mol. Catal. A 276 (2007) 47–56.
[56] R. Torviso, D. Mansilla, A. Belizan, E. Alesso, G. Moltrasio, P. Vazquez, L. Pizzio, M. Blanco, C. Caceres, Appl. Catal. A 339 (2008) 53–60.
[57] S.L. Barbosa, M.J. Dabdoub, G.R. Hurtado, S.I. Klein, A.C.M. Baroni, C. Cunha, Appl. Catal. A 313 (2006) 146–150.
[58] M. Wang, Z. Wang, Z. Sun, H. Jiang, React. Kinet. Catal. Lett. 84 (2005) 223–228.
[59] A.S. Khder, E.A. El-Sharkawy, S.A. El-Hakam, A.I. Ahmed, Catal. Commun. 9 (2008) 769–777.
[60] Y. Wang, W. Li, React. Kinet. Catal. Lett. 83 (2004) 195–203.
[61] W. Chu, X. Yang, X. Ye, Y. Wu, Appl. Catal. A 145 (1996) 125–140.
[62] P. Botella, A. Corma, J.M. Lopez-Nieto, S. Valencia, R. Jacquot, J. Catal. 195 (2000) 161–168.
[63] M.L. Kantam, K.V.S. Ranganath, M. Sateesh, K.B.S. Kumar, B.M. Choudary, J. Mol. Catal. A 225 (2005) 15–20.
[64] Y. Ma, Q.L. Wang, W. Jiang, B. Zuo, Appl. Catal. A 165 (1997) 199–206.
[65] U. Freese, F. Heinrich, F. Roessner, Catal. Today 49 (1999) 237–244.
[66] T. Mishra, Catal. Commun. 9 (2008) 21–26.